Jing, X., et al., 2021, Inverted south China: A novel configuration for Rodinia and its breakup: Geology, v. 49, https://doi.org/10.1130/G47807.1

SUPPLEMENTAL MATERIAL

Inverted South China: A novel configuration of Rodinia and its breakup

Xianqing Jing, David A. D. Evans, Zhenyu Yang, Yabo Tong, Yingchao Xu, Heng Wang

This file contains:
Supplemental text
Supplementary figures (Figures S1, S2, S3, S4)
Supplementary tables (Tables S1, S2, S3)
Supplemental references

SUPPLEMENTAL TEXT

Geological setting and paleomagnetic sampling

South China is composed of the Yangtze craton to its northwest and the Cathaysia block to its southeast. Although these two parts amalgamated during early Neoproterozic (Yao et al., 2019), the Cathaysia block was a metamorphic belt until the Mesozoic. Thus, in this paper, we prefer to use south China to represent its Yangtze craton and Cathaysia block parts, rather than South China craton

Neoproterozoic strata outcrop widely in the Three Gorges Area (TGA), Húběi Province, south China (Fig. S1). Our study area is a continuous Neoproterozoic section in Qīnglínkŏu village (QLK; 30.801°N, 110.920°E, Fig. S1). This section is located on the west limb of the Huánglíng dome, where bedding dips generally but variably westward at shallow to moderate angles. The Liántuó Fm in QLK section can be divided into lower and upper members, which are separated by a thick conglomerate layer (Fig. S1). The lower member is dominated by purple-red fine-medium sandstone. Upward, thin fine sandstone and silty shale layers are more common. Elsewhere around the TGA, Liántuó Fm overlies Huánglíng granite with a nonconformable depositional contact, but in this section, the two units are in fault contact (An et al., 2014). Previous paleomagnetic studies on the Liántuó Fm have reported sufficient results from its upper member (Jing et al., 2015), which is dated at ca. 720 Ma (Lan et al., 2015). However, the lower member, which is deposited between 780 Ma and 750 Ma (Lan et al., 2015), still lacks detailed paleomagnetic study. Therefore, we collected a total of 128 samples (12 sites) (Fig. S1) using gasoline-powered drill from the lower member (oriented with a magnetic compass). Strata in this section dip southwest at moderate angles (~40°).

Laboratory methods

All cores were cut into at least one standard specimen of 2.3 cm height and 2.54 cm diameter at Paleomagnetism Laboratory of Nanjing University. Stepwise thermal demagnetization of pilot samples was performed using an ASC-TD48 oven to isolate the characteristic remanent magnetization. After analyzing the behavior of the pilot samples, progressive thermal demagnetization was carried using 14-16 steps at a 50 or 100ºC interval for low temperatures (<550ºC), and a 20 or 30ºC interval for high temperatures up to 620ºC, and finally with a 10°C interval to 670ºC. The remanence of the specimens was measured using a 2G Enterprises Inc. cryogenic rock magnetometer (2G-755) housed in a magnetically shielded room. The remanence directions were analyzed using the principal component analysis method (Kirschvink, 1980) and the site-mean directions were calculated using Fisher spherical statistics (Fisher, 1953). Paleomagnetic software packages PMGSC (by R. Enkin), PaleoMac (Cogné, 2003) and Paleomagnetism.org (Koymans et al., 2016) were used to perform data analyses and produce related figures. GPlates software (Boyden et al., 2011) was used to reconstruct related paleogeographic figures. All the magnetic measurements were conducted at the Palaeomagnetism Laboratory of Nanjing University.

Results

Thermal demagnetization

Three remanence components are revealed by stepwise thermal demagnetization (Figure 1, S2). A low-temperature component (LTC) is separated below 400 ºC in most samples (Figure S2). The mean of LTC is Dg=359.7°, Ig=47.0°, n=109, k=44.9, α_{95}=2.2° in geographic coordinates (Figure S3A). The pole derived from the LTC (87.4°N, 296.7°E, dp/dm=1.8°/2.8°) overlaps the present north pole (Figure S3C), so the LTC is interpreted as a recent viscous remanence which records the local present field. After removal of the LTC, many samples demagnetized directly to the origin after 500 ºC (Figure 1, S2). The unblocking temperature of this high-temperature component (HTC) is 670 ºC in most samples, which implies the remanence carrier is hematite. Eight sites have an east-downward directed HTC, and one site (QLK 12) has a west-upward HTC direction (Figure 1; Table S1). The site means of HTC are Dg=78.6°, Ig=37.9°, n=9, k=83.2, α_{95}=5.7° in geographic coordinates and Ds=98.6°, Is=70.3°, n=9, k=79.3, α_{95}=5.8° in stratigraphic coordinates. The fold test of McFadden (1990) on HTC, together with results of sites LT3 and LT4 from lower member of Liántuó Formation in the east limb of Huánglíng anticline (Jing et al., 2015) are positive at 95% confidence levels. Stepwise unfolding demonstrates that the precision parameter (k) reaches its maximum at 85% but the value at 100% unfolding is insignificantly lower (Figure 1). In addition, the directions of HTC pass the reversal test (McFadden and McElhinny, 1990) at the 95% probability level (C class).

In addition, 14 samples show an intermediate-temperature component (ITC) between 400 ºC and 550-590ºC (Figure 1A). The mean direction of this component is Dg=44.0°, Ig=57.8°, n=14, k=49.9, α_{95}=6.9° in geographic coordinates (Figure S3B). The pole derived from this component (53.4°N, 176.6°E, dp/dm=7.5°/10.1°) overlaps the late Triassic pole of South China (Figure S3C), which suggests a partial late Triassic remagnetization in those samples.

Anisotropy of magnetic susceptibility (AMS)

AMS measurements on 123 samples demonstrate that their minimum axes (K3, inclination=88.6°) are mainly perpendicular to the bedding plane, while the intermediate (K2, inclination=1.0) and maximum (K1, inclination=0.9) susceptibility axes are distributed along the bedding plane in stratigraphic coordinates (Figure S4). This primary sedimentary AMS (Pares et al., 1999, Figure S4) suggests that our sampling section did not experience significant penetrative structural deformation.

SUPPLEMENTAL FIGURES

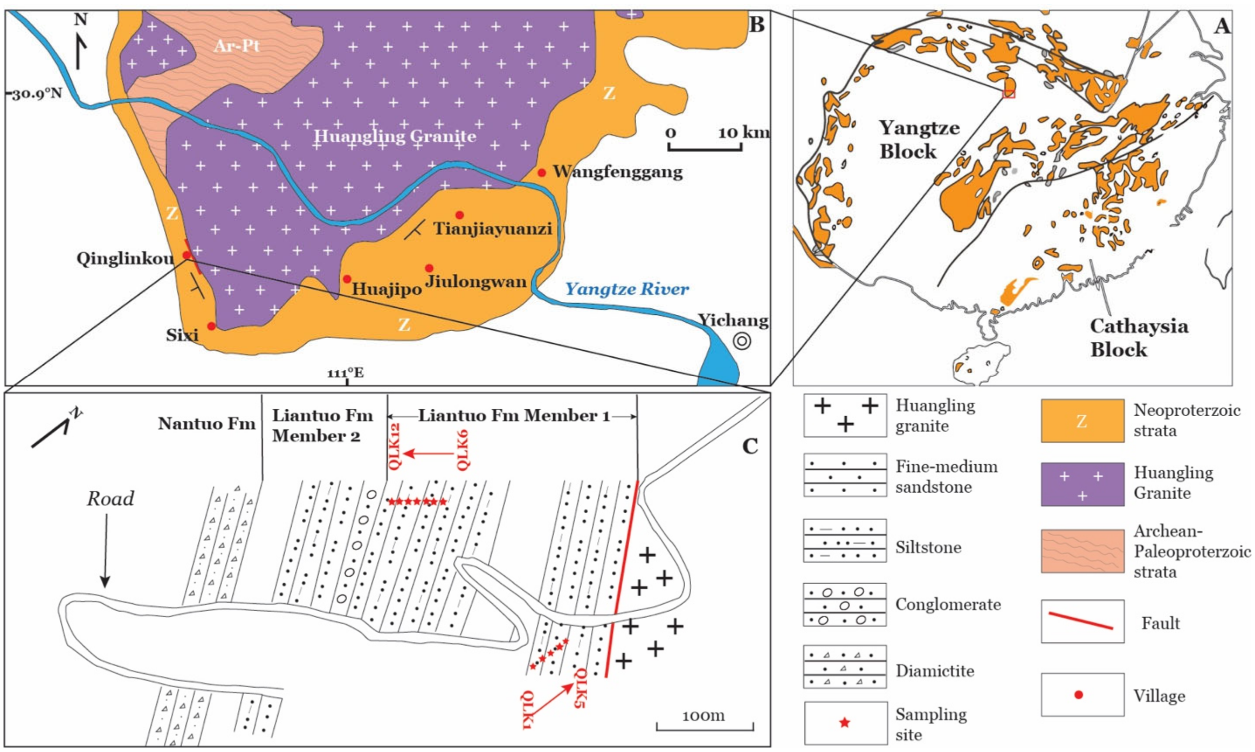

Figure S1. A: Simplified geological map showing the exposed Precambrian unit (yellow shadow area) in the South China Block. B: Simplified geological map of Three Gorges area. C: Sampling sites of Liántuó Fm distributed along the road at Qīnglínkǒu section.

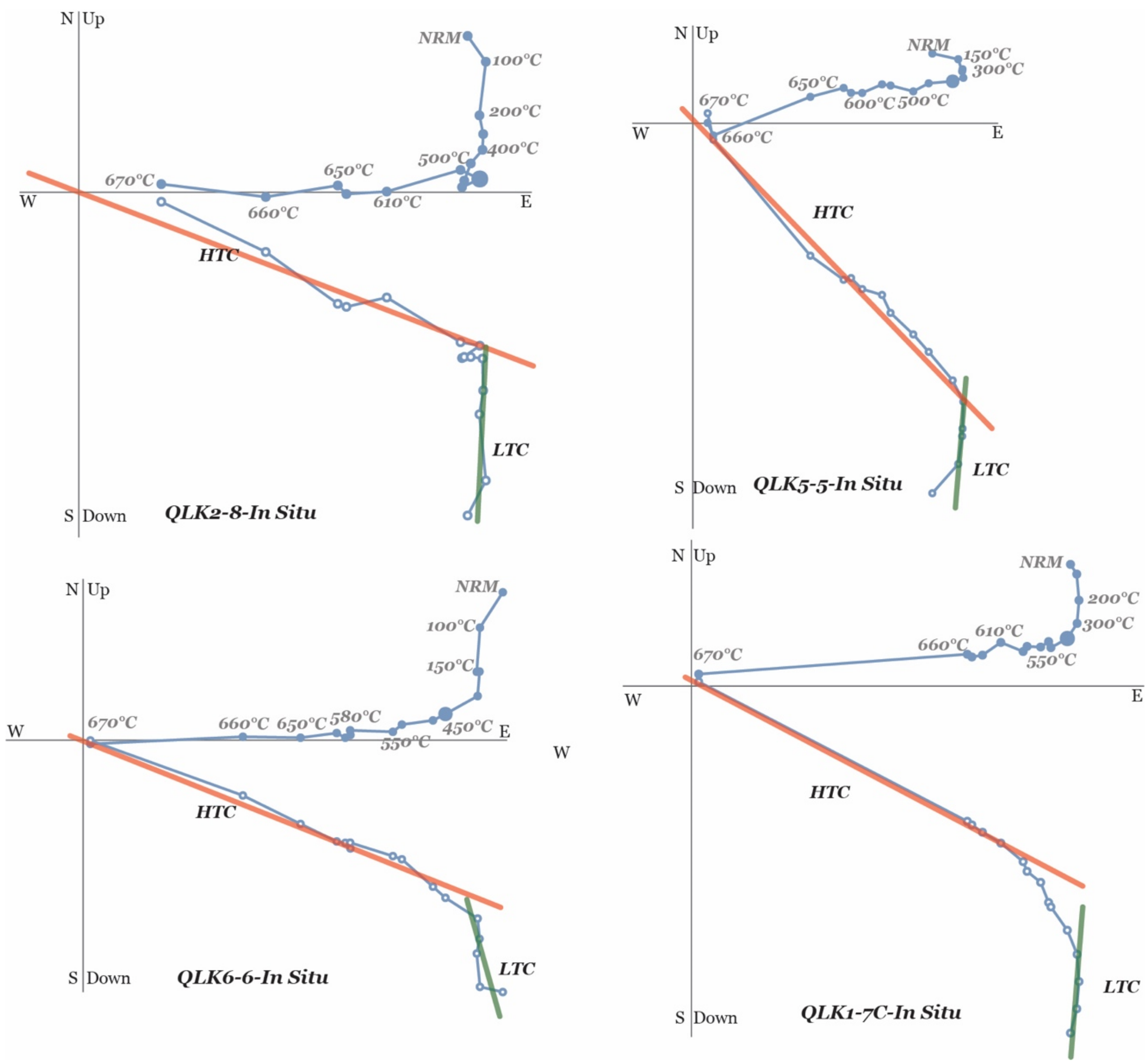

Figure S2. Orthogonal vector projection of thermal demagnetization of NRM for representative samples, in situ coordinates. Red and Green lines are fitted high temperature component (HTC) and low temperature component (LTC), respectively. Solid and open blue circles correspond to points in the horizontal (declination) and vertical (inclination) planes, respectively.

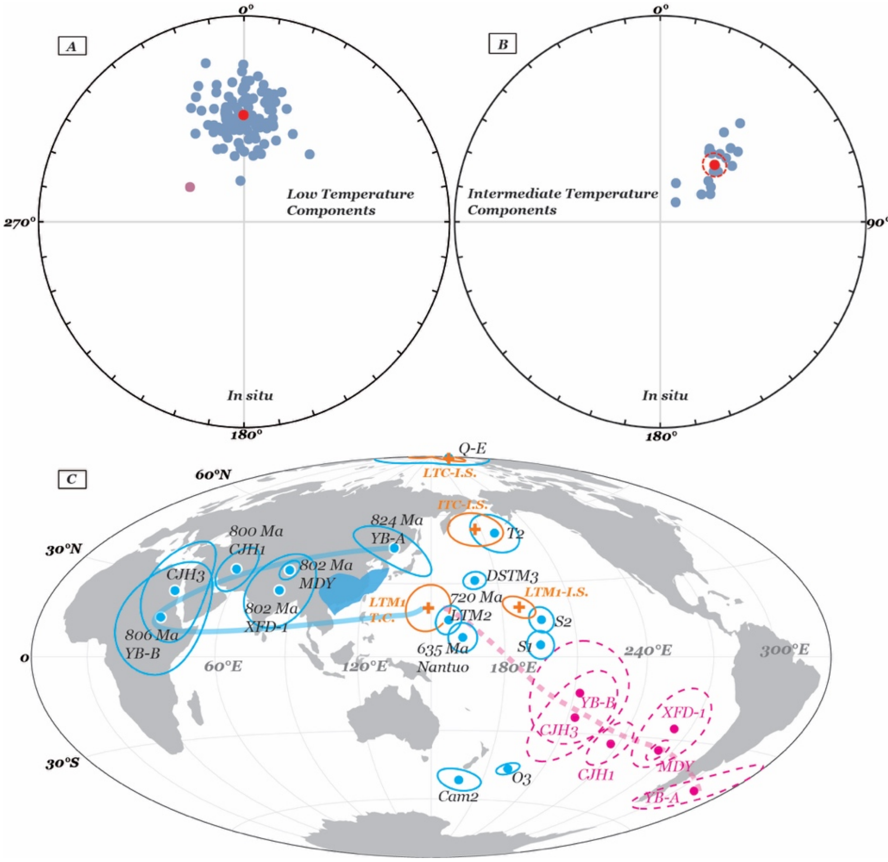

Figure S3. Equal-area stereographic projections of sample directions of the low-temperature components (A) and intermediate-temperature components (B), in situ coordinates, where filled (open) blue circles represent directions pointing down (up). Filled brown circle is a rejected sample outlier. Filled red circles are Fisher means of the samples, with the dashed red circle as 95% confidence limit. (C) Paleomagnetic poles calculated from LTC, ITC and HTC components (orange), and the existing Neoproterozoic-early Paleozoic paleopoles from the South China block shown for comparison (blue). Poles with 95% confidence ellipses (>760 Ma) are shown in the traditional interpretation of polarity (solid blue) and inverted polarity option proposed herein (dashed magenta). Coarse blue and dashed magenta lines are corresponding apparent polar wander path (APWp) options during ca. 824-720 Ma. T.C. and I.S. are tilt corrected and in situ poles. References for these poles listed in table S2 and Table 7 of Jing et al. (2018).

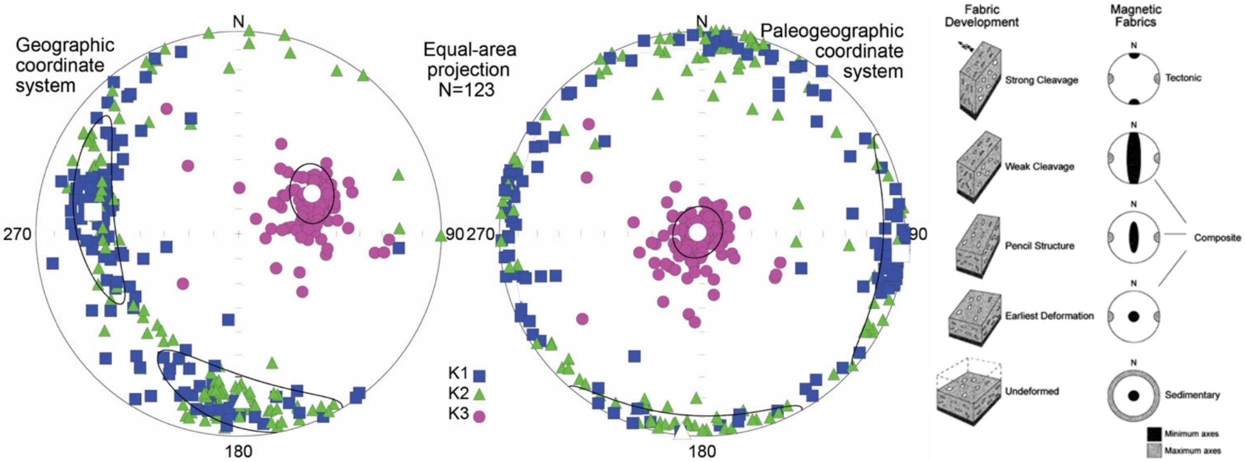

Figure S4. Equal-area and lower hemisphere projections of anisotropy of magnetic susceptibility data for the QLK sections in geographic (left) and stratigraphic (middle) coordinates. K1, K2, K3 are maximum, intermediate and minimum principal susceptibility axes. White square, triangle and circle are mean K1, K2 and K3, respectively. Also shown is the sequence of fabric development in progressively cleaved mud rocks and associated magnetic fabrics (right) from Pares et al. (1999). Magnetic fabric of our data (middle) is similar with the undeformed mud rock and a sedimentary magnetic fabric.

SUPPLEMENTAL TABLES

Table S1. High temperature component (HTC) paleomagnetic data of Liántuó Formation Lower Member from Qīnglínkǒu section, Húběi.

Sample	*n/N*	*Dg*	*Ig*	*Ds*	*Is*	*k*	
QLK1	8	87.5	34.6	110.3	65.1	28.8	10.5
QLK2	7	91.8	33.2	115.6	62.1	99.9	6.1
QLK5	7	79.7	48.6	116.7	76.4	13.7	16.9
QLK6	11	81.0	35.2	104.9	65.5	52.0	6.4
QLK7	6	68.8	39.7	84.7	73.6	24.1	13.9
QLK8	10	67.8	40.5	75.7	76.3	40.7	7.7
QLK9	5	71.0	40.0	78.3	76.9	166.0	6.0
QLK10	12	74.5	39.1	88.4	75.4	54.4	5.9
QLK12	8	262.4	-27.5	272.8	-56.5	46.7	8.2
Site mean							
	9	78.6	37.9			83.2	5.7
				98.6	70.3	79.3	5.8
Paleopole		20.1ºN, 187.5ºE, *dp/dm*=4.0º/6.7º (in situ)					
		20.0ºN, 148.7ºE, *dp/dm*=8.7º/10.0º (tilt corrected)					

N, number of sites for statistics; *n*, number of samples for statistics; *Dg*, *Ig*, *Ds*, *Is*, declination and inclination in geographic and stratigraphic coordinates; *k*, fisher precision parameter of the mean; *α95*, confidence of the mean direction; *dp/dm*, semi-axes of elliptical error around the pole at a probability of 95%.

Table S2. Summary of 830-720 Ma palaeomagnetic poles derived from major Precambrian blocks or terranes (with quality index Q>4; Van der Voo, 1990).

Stratigraphy	*Abbreviation*	*Petrology*	*Age*	*λ*	*Φ*	*dp*	*dm*	*1*	*2*	*3*	*4*	*5*	*6*	*7*	*References*
East Svalbard															
Svanbergfjellet 4 Mb	S4mb	Limestone	790	-25.9	46.8	4.3	7.7	1	0	1	1	1	0	1	***Maloof et al.,2006 Swanson-Hysell et al.,2015***
U. Grusdievbreen Fm	uGfm	Limestone	805	1.6	71.9	1.4	2.8	1	1	1	0	1	1	1	
L. Grusdievbreen Fm	lGfm	Limestone	810	-19.6	31.3	2.2	4.2	1	1	1	0	1	1	1	
South China															
Xiaofeng Dykes	XFD-1	Felsic dykes	802±10	26.1	82.1	14	15.2	1	1	1	0	1	1	1	***Jing et al., 2020***
Yanbian dyke	YB-A	Mafic dykes	824±6	45.1	130.4	19	19	1	1	1	1	0	1	1	***Niu et al.,2016***
Yanbian dyke	YB-B	Mafic dykes	806±8	14.1	32.5	20.4	20.4	1	0	1	1	0	0	1	***Niu et al.,2016***
Madiyi Fm	MDY	thick red sand	802±6	34.3	82.4	3.7	3.9	1	1	1	1	1	1	1	***Xian et al., 2020***
Chengjiang Fm	CJH1	thick red sand	800	32.8	56.3	7.1	8.6	1	1	1	1	1	1	1	***Jing et al., 2020***
Chengjiang Fm	CJH3	thick red sand	790±10	23.8	33.2	13.5	20.9	0	0	1	0	1	0	1	***Jing et al., 2020***
Liantuo Fm Member 1	LTM1	thick red sand	760	20.0	148.7	8.7	10.0	1	1	1	1	1	1	1	***This study***
Liantuo Fm Member 2	LTM2	Red mudstone	720	13.2	155.2	5.3	5.3	1	1	1	0	1	1	1	***Jing et al.,2015***
Australia															
Mundine Well dyke swarm	MDS	Mafic dykes	755±3	45.3	135.4	4.1	4.1	1	1	1	1	1	0	0	***Wingate&Giddings,2000***
Johnny's creek Member	JCM	Red siltstone	770±30	15.8	83.0	13.5	13.5	0	1	1	1	1	0	1	***Swanson-Hysell et al.,2012***
Browne Fm	Brf	Red siltstone	830-800	44.5	141.7	5.1	9	1	1	1	0	1	0	0	***Pisarevsky et al., 2007***
India															
Malani Igneous Suite	MIS	Felsic rocks	750	69.4	75.7	6.5	6.5	1	1	1	1	1	1	1	***Meert et al.,2013***
Laurentia															
Gunbarrel mafic magmatic	Gb	Mafic rocks	775	9.1	138.2	11.7	11.7	1	1	1	0	1	0	1	***Eyster et al., 2020***
Uinta Mountain Group 1	UMG1	Red siltstone	766	3.0	163.5	3.2	3.2	1	1	1	0	1	1	1	***Eyster et al., 2020***
Uinta Mountain Group 2	UMG2	Red siltstone	760	-5.8	158.7	2.7	2.7	0	1	1	0	1	0	1	***Eyster et al., 2020***
Uinta Mountain Group 3	UMG3	Red siltstone	755	4.9	160.6	3.2	3.2	0	1	1	0	1	0	1	***Eyster et al., 2020***
Nankoweap Fm	Nan	Red sandstone	760	-10.0	163.0	3.5	9.3	0	1	1	1	1	1	1	***Weil et al., 2003***
Galeros-Carbon Canyon	GCC	Sandstone	757	-0.5	166.0	9.7	9.7	1	1	1	1	1	0	1	***Eyster et al., 2020***
Kwagunt (Carbon Butte-Awatubi) combined	Kwa	Sandstone	751	14.2	163.8	3.5	3.5	1	1	1	1	1	0	1	***Eyster et al., 2020***
Franklin large igneous province	FLIP	Mafic rocks	716	8.4	163.8	2.8	2.8	1	1	1	1	1	1	0	***Denyszyn et al.,2009***

1–7, reliability criteria of Van der Voo (1990): 1-Well-dated rock age, 2-Sufficient number of samples, 3-Adequate demagnetization, 4-Field tests, 5-Structural control and tectonic coherence with craton or block involved, 6-Presence of reversals, 7-No resemblance to paleopoles of younger age. λ, latitude of the paleopoles; Φ, longitude of the paleopoles; *dp/dm*, semi-axes of elliptical error around the pole at 95% probability.

Table S3. Euler parameters for the reconstruction of Rodinia at 760 and 800 Ma. Laurentia is reconstructed relative to the absolute frame; other plates are reconstructed relative to Laurentia.

Plates	Age	Euler parameter		
		Latitude	Longitude	Angle
Laurentia	760	22.33	223.34	-100.06
Laurentia	800	22.33	223.34	-100.06
Svalbard	760	86.01	31.29	-92.10
Svalbard	800	86.01	31.29	-92.10
South China	760	-7.02	333.20	179.20
South China	800	12.65	16.92	164.03
India	760	39.96	145.56	161.24
India	800	16.84	183.46	216.68
Kalahari	760	30.98	335.60	-145.72
Kalahari	800	30.98	335.60	-145.72
Amazonia	760	14.10	313.42	-112.23
Amazonia	800	14.10	313.42	-112.23
Baltica	760	76.15	296.69	-66.93
Baltica	800	76.15	296.69	-66.93
Siberia	760	74.35	132.05	-166.44
Siberia	800	74.35	132.05	-166.44
Australia	760	-27.37	323.22	-127.09
Australia	800	-27.37	323.22	-127.09
Tarim	760	69.52	348.68	116.31
Tarim	800	69.52	348.68	116.31

SUPPLEMENTAL REFEERENCES

An, Z., Tong, J., Ye, Q., Tian, L., Song, H., and Zhao, X., 2014, Neoproterozoic Stratigraphic Sequence and Sedimentary Evolution at Qinglinkou Section, East Yangtze Gorges Area: Earth Science-Journal of China University of Geoscience(in Chinese), v. 39.

Boyden, J.A., Müller, R.D., Gurnis, M., Torsvik, T.H., Clark, J.A., Turner, M., Ivey-Law, H., Watson, R.J., and Cannon, J.S., 2011, Next-generation plate-tectonic reconstructions using GPlates, *in* Keller, G.R. and Baru, C. eds., Geoinformatics, Cambridge, Cambridge University Press, p. 95–114, doi:10.1017/CBO9780511976308.008.

Cogné, J.P., 2003, PaleoMac: A Macintosh^{TM} application for treating paleomagnetic data and making plate reconstructions: Geochemistry, Geophysics, Geosystems, v. 4, p. 1–8, doi:10.1029/2001GC000227.

Denyszyn, S.W., Halls, H.C., Davis, D.W., and Evans, D. a. D., 2009, Paleomagnetism and U-Pb geochronology of Franklin dykes in High Arctic Canada and Greenland: a revised age and paleomagnetic pole constraining block rotations in the Nares Strait region: Canadian

Journal of Earth Sciences, v. 46, p. 689–705, doi:10.1139/E09-042.
Eyster, A., Weiss, B.P., Karlstrom, K., and Macdonald, F.A., 2019, Paleomagnetism of the Chuar Group and evaluation of the late Tonian Laurentian apparent polar wander path with implications for the makeup and breakup of Rodinia: GSA Bulletin, doi:10.1130/B32012.1.
Fisher, R., 1953, Dispersion on a Sphere: Proceedings of the Royal Society A: Mathematical, Physical and Engineering Sciences, v. 217, p. 295–305, doi:10.1098/rspa.1953.0064.
Jing, X., Yang, Z., Evans, D.A.D., Tong, Y., Xu, Y., and Wang, H., 2020, A pan-latitudinal Rodinia in the Tonian true polar wander frame: Earth and Planetary Science Letters, v. 530, p. 115880, doi:10.1016/j.epsl.2019.115880.
Jing, X., Yang, Z., Tong, Y., and Han, Z., 2015, A revised paleomagnetic pole from the mid-Neoproterozoic Liantuo Formation in the Yangtze block and its paleogeographic implications: Precambrian Research, v. 268, doi:10.1016/j.precamres.2015.07.007.
Jing, X., Yang, Z., Tong, Y., Wang, H., and Xu, Y., 2018, Identification of multiple magnetizations of the Ediacaran strata in South China: Geophysical Journal International, v. 212, p. 54–75, doi:10.1093/gji/ggx396.
Kirschvink, J.L., 1980, The least-squares line and plane and the analysis of palaeomagnetic data: Geophysical Journal International, v. 62, p. 699–718, doi:10.1111/j.1365-246X.1980.tb02601.x.
Koymans, M.R., Langereis, C.G., Pastor-Galán, D., and van Hinsbergen, D.J.J., 2016, Paleomagnetism.org: An online multi-platform open source environment for paleomagnetic data analysis: Computers and Geosciences, v. 93, p. 127–137, doi:10.1016/j.cageo.2016.05.007.
Lan, Z., Li, X.H., Zhu, M., Zhang, Q., and Li, Q.L., 2015, Revisiting the Liantuo Formation in Yangtze Block, South China: SIMS U-Pb zircon age constraints and regional and global significance: Precambrian Research, v. 263, p. 123–141, doi:10.1016/j.precamres.2015.03.012.
Maloof, A.C., Halverson, G.P., Kirschvink, J.L., Schrag, D.P., Weiss, B.P., and Hoffman, P.F., 2006, Combined paleomagnetic, isotopic, and stratigraphic evidence for true polar wander from the Neoproterozoic Akademikerbreen Group, Svalbard, Norway: Bulletin of the Geological Society of America, v. 118, p. 1099–1124, doi:10.1130/B25892.1.
McElhinny, M.W., 1964, Statistical Significance of the Fold Test in Palaeomagnetism: Geophysical Journal of the Royal Astronomical Society, v. 8, p. 338–340, doi:10.1111/j.1365-246X.1964.tb06300.x.
McFadden, P.L., 1990, A new fold test for palaeomagnetic studies: Geophysical Journal International, v. 103, p. 163–169, doi:10.1111/j.1365-246X.1990.tb01761.x.
McFadden, P.L., and Lowes, F.J., 1981, The discrimination of mean directions drawn from Fisher distributions: Geophysical Journal of the Royal Astronomical Society, v. 67, p. 19–33, doi:10.1111/j.1365-246X.1981.tb02729.x.
McFadden, P.L., and McElhinny, M.W., 1990, Classification of the reversals test in palaeomagnetism: Geophysical Journal International, v. 103, p. 725–729.

Meert, J.G., Pandit, M.K., and Kamenov, G.D., 2013, Further geochronological and paleomagnetic constraints on Malani (and pre-Malani) magmatism in NW India: Tectonophysics, v. 608, p. 1254–1267, doi:10.1016/j.tecto.2013.06.019.

Niu, J., Li, Z.-X., and Zhu, W., 2016, Palaeomagnetism and geochronology of mid-Neoproterozoic Yanbian dykes, South China: implications for a c. 820–800 Ma true polar wander event and the reconstruction of Rodinia: Geological Society, London, Special Publications, v. 424, p. 191–211, doi:10.1144/SP424.11.

Pares, J.P., Van Der Pluijm, B.A., and Dinarès-Turell, J., 1999, Evolution of magnetic fabric during incipient deformation of mudrock (Pyrenees, northen Spain): Tectonophysics, v. 307, p. 1–14.

Pisarevsky, S.A., Wingate, M.T.D., Stevens, M.K., and Haines, P.W., 2007, Palaeomagnetic results from the Lancer 1 stratigraphic drillhole, Officer Basin, Western Australia, and implications for Rodinia reconstructions: Australian Journal of Earth Sciences, v. 54, p. 561–572, doi:10.1080/08120090701188962.

Swanson-Hysell, N.L., Maloof, A.C., Condon, D.J., Jenkin, G.R.T., Alene, M., Tremblay, M.M., Tesema, T., Rooney, A.D., and Haileab, B., 2015, Stratigraphy and geochronology of the Tambien Group, Ethiopia: Evidence for globally synchronous carbon isotope change in the Neoproterozoic: Geology, v. 43, p. 323–326, doi:10.1130/G36347.1.

Swanson-Hysell, N.L., Maloof, A.C., Kirschvink, J.L., Evans, D.A.D., Halverson, G.P., and Hurtgen, M.T., 2012, Constraints on neoproterozoic paleogeography and paleozoic orogenesis from paleomagnetic records of the bitter springs formation, amadeus basin, central Australia: American Journal of Science, v. 312, p. 817–884, doi:10.2475/08.2012.01.

Van der Voo, R., 1990, The reliability of paleomagnetic data: Tectonophysics, v. 184, p. 1–9, doi:10.1016/0040-1951(90)90116-P.

Weil, A.B., Geissman, J.W., Heizler, M., and Van der Voo, R., 2003, Paleomagnetism of Middle Proterozoic mafic intrusions and Upper Proterozoic (Nankoweap) red beds from the Lower Grand Canyon Supergroup, Arizona: Tectonophysics, v. 375, p. 199–220, doi:10.1016/S0040-1951(03)00339-1.

Wingate, M.T.D., and Giddings, J.W., 2000, Age and palaeomagnetism of the MundineWell dyke swarm, Western Australia: implications for an Australia–Laurentia connection at 755 Ma: Precambrian Research, v. 100, p. 335–357.

Xian, H., Zhang, S., Li, H., Yang, T., and Wu, H., 2020, Geochronological and palaeomagnetic investigation of the Madiyi Formation, lower Banxi Group, South China: Implications for Rodinia reconstruction: Precambrian Research, v. 336, doi:10.1016/j.precamres.2019.105494.

Yao, J., Cawood, P.A., Shu, L., and Zhao, G., 2019, Jiangnan Orogen, South China: A ~970–820 Ma Rodinia margin accretionary belt: Earth-Science Reviews, v. 196, p. 102872, doi:10.1016/j.earscirev.2019.05.016